A geometrically inspired model for brittle damage in compressible elastomers

Sanhita Das
Research Scholar,
Centre of Excellence
in Advanced Mechanics of Materials,
Department of Civil Engineering;
Indian Institute of Science,
Bangalore 560012,
India Email: sanhitadas@iisc.ac.in

Shubham Sharma
Research Scholar,
Centre of Excellence
in Advanced Mechanics of Materials,
Department of Civil Engineering;
Indian Institute of Science,
Bangalore 560012,India
Email: shubhamsharm@iisc.ac.in

Ananth Ramaswamy
Professor,
Centre of Excellence
in Advanced Mechanics of Materials,
Department of Civil Engineering;
Indian Institute of Science,
Bangalore 560012,India
Email: ananth@iisc.ac.in

Debasish Roy
Professor,
Centre of Excellence
in Advanced Mechanics of Materials,
Department of Civil Engineering;
Indian Institute of Science,
Bangalore 560012,India
Email: royd@iisc.ac.in

J. N. Reddy*
Distinguished Professor,
J. Mike Walker Department of Mechanical Engineering
Texas A&M University,
College Station, 77843-3123
Email: jnreddy@tamu.edu

ABSTRACT

Regularised continuum damage models such as those based on an order parameter (phase field) have been extensively used to characterise brittle damage of compressible elastomers. However, the prescription of the surface integral and the degradation function for stiffness lacks a physical basis. In this article we propose a continuum damage model

*Address all correspondence to this author.

that draws upon the postulate that a damaged material could be mathematically described as a Riemannian manifold. Working within this framework with a well defined Riemannian metric designed to capture features of isotropic damage, we prescribe a scheme to prevent damage evolution under pure compression. The result is a substantively reduced stiffness degradation due to damage before the peak response and a faster convergence rate with the length scale parameter in comparison with a second order phase field formulation that involves a quadratic degradation function. We also validate this model using results of tensile experiments on double notched plates.

INTRODUCTION

Prediction of damage in hyperelastic polymers is of immense interest from both industrial and research standpoints. Of the myriad mechanical responses that polymers exhibit under varying strain rates and temperatures, brittle damage following a linear elastic response is the characteristic of a slow deformation process which does not allow for viscous response prior to failure. [1]

Several approaches to modelling damage which represent cracks as discrete objects are available, Linear Elastic Fracture Mechanics (LEFM) and Cohesive Zone Modelling (CZM) to wit. But extensions of these theories to boundary value problems of higher dimensions have proved to be tedious due to the criteria-based evolution of discontinuity in the displacement field. Regularised [2] and non-regularised continuum approaches eliminate the necessity of such criteria and redefinition of the mesh to account for the evolving discontinuity [3]. A widely implemented regularised continuum model for damage is the phase-field based variational approach which involves minimisation of a global energy functional. The model involves solving a set of partial differential equations which govern the nucleation and propagation of cracks in a robust and fairly accurate manner [1, 4–6]. However, there are some limitations with the second order, phase-field damage model with quadratic degradation function [1]. One of them is the premature stiffness degradation observed prior to damage initiation which leads to non-linearity in an otherwise linear elastic response [3, 7, 8]. The other is the need to introduce higher order derivatives in order to improve computational efficiency. [3, 9]. By way of a fix for the first issue, higher order degradation

functions have been used [3, 7], which have yielded plausible responses for special cases such as brutal damage. To overcome the second limitation, these higher order derivatives, proposed ad-hoc and hence generally lacking in a rigorous basis, require higher degrees of approximation making the finite element implementation more tedious and computationally expensive. Specifically in the context of brittle fracture in hyperelastic materials, the tension-compression energy decomposition is different from [4] due to finite deformation. This aspect has been of interest to several researchers [10–12] who suggest some innovative approaches. However, they either lack seamlessness or they consider the split on the basis of positiveness of the principal stretch which includes both volumetric and deviatoric responses.

The enhancements to the classical second-order phase field formulation ([5, 6, 13]) enable a better correspondence with the physicality of brittle damage. The spatial derivatives and the degradation functions in both the classical and the enhanced phasefield approaches however stem from the requirements of numerical accuracy and faster convergence. These approaches no doubt reconcile with the traditional Griffith's theory on fracture by demonstrating that the surface energy converges to fracture toughness on reducing the regularisation length scale to zero. However, if regularisation could be introduced in a geometrically meaningful way, one could reap the added advantages of physical transparency (thus enabling easier reconciliation with experiments) and, perhaps, faster convergence too. Guided by this thought, we, in this article, propose a physically inspired isotropic damage model on the basis of the hypothesis that damage introduces a non-zero Riemannian curvature into the undeformed and undamaged Euclidean body. Thus the surface energy that is required for damage to initiate and propagate must be a function of this curvature. Moreover, in order to distinguish the contributions of tensile and compressive strain energies to damage propagation in compressible hyperelastic materials, we propose a novel scheme of energy decomposition which demonstrates seamlessness across the tension-compression divide [11] whilst conforming to the notion that damage propagation is infeasible under pure compression [10, 12].

In Section (1) of the article, we describe the various configurations and essentials of Riemannian geometry with the development of the relevant kinematic quantities. Section 2 deals with the

geometry inspired modified strain energy. It also contains the derivation of the Ricci curvature and the surface energy. Section 3 devoted to the development of the microforce and the macroforce balance laws, following which the constitutive theory is derived in Section 4. The implementation of the theory for problems involving homogeneous, one dimensional and two dimensional bodies is carried out in the Section 5. Finally some concluding remarks are presented in Section 5.3.

1 KINEMATICS OF THE DAMAGED UNDEFORMED AND DEFORMED RIEMANNIAN MANIFOLDS

Continuum damage models inspired by physical or geometric considerations such as [14–16] typically employ a damage variable which is a measure of the reduction in area that can effectively capture the so called stiffness degradation of the material. On similar lines, damage in a hyperelastic rubbery material should entail a reduction in the surface area over which the polymer chains contribute to material stiffness. This reduction in area and the attendant emergence of incompatibilities could be modelled by considering the material body (manifold) to undergo a smooth transformation from Euclidean to Riemannian [17]. The metric tensors associated with the two manifolds thus must capture, among others, the change in the area measure. A simple way to arrive at the metric of a damaged manifold could be by scaling the Euclidean metric by a scalar function that involves the ratio of effective surface areas after and before damage. In order to account for deformation as well, we may define three material configurations as in figure 1, viz. the referential (or undamaged and undeformed) configuration $\mathcal{B}$, the damaged and undeformed configuration $\mathcal{C}$ and the damaged and deformed configuration $\mathcal{S}$. Note that, in our current worldview, $\mathcal{B}$ is Euclidean while $\mathcal{C}$ and $\mathcal{S}$ are Riemannian.

Further, we assume the existence of a smooth (diffeomorphic) map ϕ taking points from the reference to the deformed and damaged configuration. It is interpreted as a composition of two smooth maps ϕ_d and ϕ_M defined by,

$$\phi_d : \mathcal{B} \to \mathcal{C} \tag{1}$$

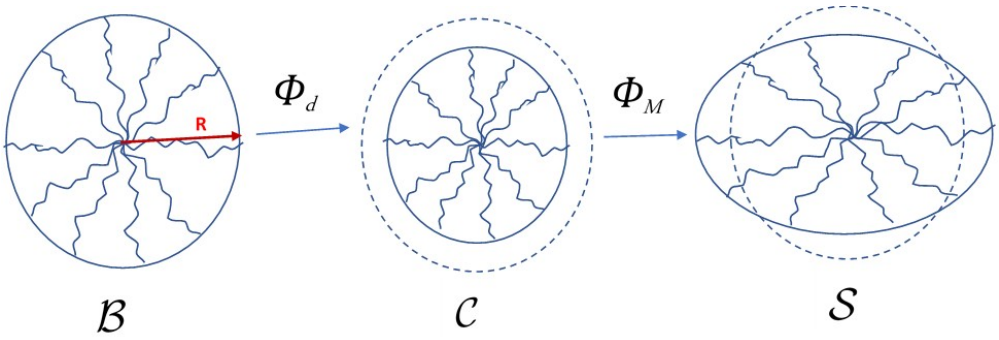

Fig. 1. Schematic figure of the three configurations and the deformation maps

$$\phi_M : \mathcal{C} \to \mathcal{S} \tag{2}$$

The corresponding tangent maps or deformation gradients are denoted by $\mathbf{F_d}$ and $\mathbf{F_M}$ respectively.

$$\mathbf{F} = \mathbf{F}_M \mathbf{F}_d \tag{3}$$

We assume ϕ_d to be an identity map; thus the associated deformation gradient $\mathbf{F}_d$ mapping the respective tangent spaces is identity too, which also permits us to take the co-ordinate bases as identical. Thus Eqn. (3) simplifies to

$$\mathbf{F} = \mathbf{F}_M \tag{4}$$

Associated with the manifolds $\mathcal{B}$, $\mathcal{C}$ and $\mathcal{S}$ are the respective metric tensors $\mathbf{G}$, $\mathbf{G}_d$ and $\mathbf{g}_d$. While $\mathbf{G}$ is the standard Euclidean metric of the reference body, the undeformed and deformed Riemannian metrics $\mathbf{G}_d$ and $\mathbf{g}_d$ may be expressed as functions of the undeformed and deformed

Euclidean configurations (fictitious ones without any geometric incompatibility) as follows:

$$\mathbf{G}_d = f(D)\mathbf{G} \tag{5}$$

$$\mathbf{g}_d = f(D)\mathbf{g} \tag{6}$$

Here $\mathbf{G}$ and $\mathbf{g}$ are Euclidean metrics of the undamaged undeformed and undamaged deformed configurations and $f(D)$ is a scaling factor, a measure of the ratio of the effective undamaged area to the area prior to damage. In [14–16], the scaling factor is chosen as $(1-D)^2$. As will be shown subsequently, such a choice in our case where the evolution of damage is derived from minimization of the total internal energy, leads to high non-linearity prior to damage initiation which is non-physical. Thus we choose the function $f(D)$ to assume the form $f(D) = (1-D)$, where D is an internal variable. Pulled back to the undeformed undamaged configuration, one can write the right Cauchy Green tensor associated with the deformation as,

$$\mathbf{C}_d = f(D)\mathbf{F}^T\mathbf{g}\mathbf{F} \tag{7}$$

where we make use of Eqn. (4).

We now appeal to Miehe's microsphere model [13] to determine the homogenised strain measure of a single representative chain. This strain measure needs to be modified for damage in the sense that homogenisation must now be carried out over the area remaining after damage, an aspect that has not been taken into account so far [1]. The stretch of the chains used in the process of homogenisation must therefore be calculated using the pulled back Riemannian metric instead of the undamaged Euclidean metric. The homogenised stretch in the damaged

undeformed configuration is given as,

$$\Lambda_{d0}^2 = \frac{\int_{A_0} \mathbf{R}.\mathbf{G}_d\mathbf{R}dA_0}{\int_{A_0} dA_0} \tag{8}$$

where A_0 is the surface area of the undeformed undamaged microsphere and $\mathbf{R}$ is the position vector, i.e. the one joining the two ends of the chain. Implementing the explicit expression for $\mathbf{G}_d$ in Eqn. (8) one obtains,

$$\Lambda_{d0}^2 = (1 - D) \tag{9}$$

Similarly the homogenised stretch in the deformed configuration is given by,

$$\Lambda_{d}^2 = \frac{\int_{A_0} \mathbf{R}.\mathbf{C}_d\mathbf{R}dA_0}{\int_{A_0} dA_0} \tag{10}$$

Eqn. (10) simplifies to,

$$\Lambda_{d}^2 = \frac{(1 - D)}{3} tr(\mathbf{C}) \tag{11}$$

where $\mathbf{C} = \mathbf{F}^T\mathbf{g}\mathbf{F}$.

The infinitesimal area measure of the damaged undeformed configuration dA_d may be obtained using the reduced metric tensors of the undamaged and damaged configurations, $\mathbf{G}^{surf}$

and $\mathbf{G}_d^{surf}$ respectively, via:

$$dA_d = \frac{\sqrt{det(\mathbf{G}_d^{surf})}d\Phi d\Theta}{\sqrt{det(\mathbf{G}^{surf})}d\Phi d\Theta}dA_0 \tag{12}$$

where Θ and Φ correspond to referential spherical coordinates. Using the scaling function, the last equation may be simplified to,

$$dA_d = (1-D)dA_0 \tag{13}$$

For compressible solids, the volume measures for the undeformed and deformed damaged configurations in material coordinates must be obtained. For the undeformed damaged manifold, we have the following Jacobian:

$$J_{d0} = \sqrt{\frac{det(\mathbf{G_d})}{det(\mathbf{G})}} = (1-D)^{\frac{3}{2}} \tag{14}$$

and for the deformed damaged manifold, the same is given by,

$$J_d = \sqrt{\frac{det(\mathbf{C_d})}{det(\mathbf{G})}} = (1-D)^{\frac{3}{2}}\sqrt{det(\mathbf{F}^T\mathbf{F})} \tag{15}$$

The curvature associated with the damaged undeformed manifold is of special relevance in this work and it is determined in Section 2.3.

2 GEOMETRY INSPIRED FREE ENERGY FOR DAMAGED SOLID

The evolving damage opens up internal surfaces within the body manifold, warranting appropriate modifications in the free energy consistent with our geometric setup.

2.1 Free energy of undamaged hyperelastic solid

For an undamaged incompressible hyperelastic solid, the free energy is given by the conventional inverse Langevin form (see [18]), the expression for which is,

$$\begin{aligned}\psi = \hat{\psi}(\mathbf{C},\theta) =& k_B n N \theta \Bigg[\Lambda^r \mathscr{L}^{-1}(\Lambda^r) \\ &+ \ln \frac{\mathscr{L}^{-1}(\Lambda^r)}{\sinh(\mathscr{L}^{-1}(\Lambda^r))} - f(\Lambda^r_{ref}) \Bigg]\end{aligned} \tag{16}$$

where, $\Lambda^r = \frac{\Lambda}{N}$, $\Lambda = \frac{1}{3} tr(\mathbf{C})^{1/2}$, Λ^r_{ref} is the reference strain and $f(\Lambda) = \Lambda \mathscr{L}^{-1}(\Lambda) + \ln \frac{\mathscr{L}^{-1}(\Lambda)}{\sinh(\mathscr{L}^{-1}(\Lambda))}$ in the reference undeformed configuration

For compressible solids, the free energy takes on the following form,

$$\begin{aligned}\psi = \hat{\psi}(\mathbf{C},\theta) =& k_B n N \theta \Bigg[\overline{\Lambda}^r \mathscr{L}^{-1}(\overline{\Lambda}^r) + \ln \frac{\mathscr{L}^{-1}(\overline{\Lambda}^r)}{\sinh(\mathscr{L}^{-1}(\overline{\Lambda}^r))} \\ &- f(\overline{\Lambda}^r_{ref}) \Bigg] + K(J - J_{ref})^2\end{aligned} \tag{17}$$

where, $\overline{\Lambda}^r = \frac{\overline{\Lambda}}{N}$, $\overline{\Lambda} = J^{-\frac{1}{3}} \frac{1}{3} tr(\mathbf{C})^{1/2}$, $J = \frac{\sqrt{detg}}{\sqrt{detG}} det\mathbf{F}$, $J_{ref} = 1$ and $\overline{\Lambda}^r_{ref}$ is deviatoric reference strain.

2.2 Modification in strain energy

Thus for compressible solids, the strain energy due to conformal stretching of polymer chains is specified by,

$$\begin{aligned}\psi_e = \hat{\psi}_e(\mathbf{C},\theta) =& k_B n_d N \theta \Bigg[\overline{\Lambda}^r_d \mathscr{L}^{-1}(\overline{\Lambda}^r_d) + \ln \frac{\mathscr{L}^{-1}(\overline{\Lambda}^r_d)}{\sinh(\mathscr{L}^{-1}(\overline{\Lambda}^r_d))} \\ &- f(\overline{\Lambda}^r_{d0}) \Bigg] + \frac{K}{2}(J_d^{0.5} - J_{d0}^{0.5})^2\end{aligned} \tag{18}$$

where $\overline{\Lambda}_d^r = \frac{\overline{\Lambda}_d}{\sqrt{N}}$, $\overline{\Lambda}_d = J_d^{-\frac{1}{3}} \frac{1}{\sqrt{3}} tr(\mathbf{C}_d)^{1/2} = J^{-\frac{1}{3}} \frac{1}{\sqrt{3}} tr(\mathbf{C})^{1/2}$, and $J = \sqrt{det \mathbf{F^T g F}}$ n_d is the number density of chains in the deformed damaged configuration expressed in material coordinates. Hence, $n_d = n(1-D)^{1.5}$.

Under pure compression, no damage takes place. Accordingly, the free energy must include a provision to eliminate degradation of the stiffness of the material under pure compression. Similar to [10, 12], we degrade only the deviatoric and the tensile parts of the volumetric strain energy. In deriving the following equation for the modified strain energy, we make use of the damaged, undeformed and deformed kinematic quantities introduced in Section (1),

$$\begin{aligned} \psi_e =& \hat{\psi}_e(\mathbf{C}, \theta) = k_B n (1-D)^{1.5} N \theta \Bigg[\overline{\Lambda}_d^r \mathscr{L}^{-1}(\overline{\Lambda}_d^r) \\ & + \ln \frac{\mathscr{L}^{-1}(\overline{\Lambda}_d^r)}{\sinh(\mathscr{L}^{-1}(\overline{\Lambda}_d^r))} - f(\overline{\Lambda}_{d0}^r) \Bigg] \\ & + \frac{K}{2}(J_d^{0.5} - J_{d0}^{0.5})^2 H(J-1) + \frac{K}{2}(J^{0.5}-1)^2 H(1-J) \end{aligned} \tag{19}$$

where $H(J-1)$ denotes the Heaviside step function.

2.3 Curvature based surface energy

A part of the strain energy due to bond stretching is expended in order to create new surfaces; it may be assumed to be depend on the Ricci curvature R_d of the damaged Riemannian manifold prior to mechanical deformation induced by the map ϕ.

The energy to create surfaces which is denoted by ψ_{R_d} has thus the following functional form,

$$\psi_{R_d} = \hat{\psi}_{R_d}(R_d, D) \tag{20}$$

R_d is a function of the Christoffel symbols associated with the Levi-Civita connection for the undeformed damaged manifold introduced in the section (1). The expression for the connection may

be derived from the compatibility condition associated with the manifold and is given by,

$$\nabla_\alpha G_{d|\mu\nu} = 0 \tag{21}$$

The Christoffel symbols in the indicial notation assume the following form,

$$\Gamma^L_{dMI} = \frac{1}{2} G^{KL}_d \left[G_{dIK,M} + G_{dKM,I} - G_{dMI,K} \right] \tag{22}$$

The last equation may be simplified as:

$$\Gamma^L_{dMI} = \frac{1}{2(1-D)} G^{KL}_d \left[G_{IK} D_{,M} + G_{KM} D_{,I} - G_{MI} D_{,K} \right] \tag{23}$$

The curvature tensor $\hat{\mathbf{R}}$ is related to the metric and the connection as follows,

$$\hat{\mathbf{R}}^L_{IKJ} = \partial_K \Gamma^L_{dJI} - \partial_J \Gamma^L_{dKI} + \Gamma^L_{dKA} \Gamma^A_{dJI} + \Gamma^L_{dJA} \Gamma^A_{dKI} \tag{24}$$

where $\hat{\mathbf{R}}^L_{IKJ}$ denote the components of $\hat{\mathbf{R}}$. The components of the Ricci tensor $\hat{\mathbf{R}}_d$ are on the other hand given by contraction of the curvature tensor,

$$\hat{\mathbf{R}}_{dIJ} = \hat{\mathbf{R}}^K_{IKJ} = \partial_K \Gamma^K_{dJI} - \partial_J \Gamma^K_{dKI} + \Gamma^K_{dKA} \Gamma^A_{dJI} + \Gamma^K_{dJA} \Gamma^A_{dKI} \tag{25}$$

By definition, the Ricci scalar curvature is the result of contraction of the two lower indices in

the Ricci tensor and is given by,

$$R_d = \mathbf{G_d}^{IJ}\hat{\mathbf{R}}_{dIJ} \tag{26}$$

The expression above may be simplified to:

$$R_d(D, \nabla D, \Delta D) = -\frac{2}{(1-D)^2}G^{JI}D_{,IJ} + \frac{3}{2(1-D)^3}G^{IJ}D_{,I}D_{,J} \tag{27}$$

Expressed in material coordinates, we have:

$$R_d(D, \nabla D, \Delta D) = -\frac{2}{(1-D)^2}\Delta D + \frac{3}{2(1-D)^3}\nabla D \cdot \nabla D \tag{28}$$

It is important to observe that the curvature might be negative and that it tends to infinity as D approaches 1, which is indicative of a singularity consistent with the physical understanding of damage; ψ_{R_d} associated with damage evolution, however, must be positive definite and finite. It must also conform to the fact that $D = 0$ corresponds to an extremum for the potential. We postulate the following expression for ψ_{R_d} which involves a term quadratic in damage.

$$\begin{aligned}\psi_{R_d} &= \frac{12}{11\sqrt{3}}M\left(D^2 + \frac{1}{2}l_R^2 det(\mathbf{G}_d)R_d\right) \\ &= \frac{12}{11\sqrt{3}}M\left(D^2 + l_R^2\left[\frac{3}{4}\nabla D \cdot \nabla D - (1-D)\Delta D\right]\right)\end{aligned} \tag{29}$$

where M is a material constant that quantifies the resistivity of the material to damage and hence the curvature. l_R is a length scale over which the curvature is expected to be highly deviating from 0. The term $\frac{1}{2}Ml_R^2 det(\mathbf{G}_d)$ may be thus interpreted as a resistive pressure that preserves the integrity of the material.

2.4 Modified free energy of the damaged deformed solid

The total free energy is thus given by,

$$\begin{aligned}\psi = \psi_{R_d} + \psi_e = \frac{12}{11\sqrt{3}} M \left(D^2 + l_R^2 \left[\frac{3}{4} \nabla D \cdot \nabla D - (1-D) \Delta D \right] \right) \\ + \mu (1-D)^{1.5} \left(\overline{\Lambda}_d^r \mathscr{L}^{-1}(\overline{\Lambda}_d^r) + \ln \frac{\mathscr{L}^{-1}(\overline{\Lambda}_d^r)}{\sinh(\mathscr{L}^{-1}(\overline{\Lambda}_d^r))} - f(\overline{\Lambda}_{d0}^r) \right) \\ + \frac{K}{2} (J_d^{0.5} - J_{d0}^{0.5})^2 H(J-1) + \frac{K}{2} (J^{0.5} - 1)^2 H(1-J)\end{aligned} \tag{30}$$

Implementing a smooth approximation to the Heaviside step function, the free energy assumes the form,

$$\begin{aligned}\psi = & \frac{12}{11\sqrt{3}} M \left(D^2 + l_R^2 \left[\frac{3}{4} \nabla D \cdot \nabla D - (1-D) \Delta D \right] \right) \\ & + \mu (1-D)^{1.5} \left(\overline{\Lambda}_d^r \mathscr{L}^{-1}(\overline{\Lambda}_d^r) + \ln \frac{\mathscr{L}^{-1}(\overline{\Lambda}_d^r)}{\sinh(\mathscr{L}^{-1}(\overline{\Lambda}_d^r))} - f(\overline{\Lambda}_{d0}^r) \right) \\ & + \frac{K}{4} (J_d^{0.5} - J_{d0}^{0.5})^2 (1 + \tanh \beta (J-1)) \\ & + \frac{K}{4} (J^{0.5} - 1)^2 (1 + \tanh \beta (1-J))\end{aligned} \tag{31}$$

where $\mu = k_B N n \theta$ and β is a very large number.

3 MACROFORCE AND MICROFORCE BALANCES

We use the principle of virtual power to derive the macroforce and microforce balance laws. The external power is defined as,

$$\delta W_{ext} = \int_{\partial V_0} (\mathbf{t} \cdot \delta \dot{\phi} + \chi \delta \dot{D}) dA_0 + \int_{V_0} \mathbf{b} \cdot \delta \dot{\phi} dV_0 \tag{32}$$

and the internal power is given by,

$$\delta W_{int} = \int_{V_0} \mathbf{P} : \delta\nabla_X \dot{\phi} + \xi \cdot \delta\nabla\dot{D} + \pi\delta\dot{D} + \kappa\delta\dot{\Delta D} dV_0 \tag{33}$$

where π, ξ and κ are the driving forces dual to D, $\nabla\dot{D}$, and ΔD, respectively.

Equating the external and internal virtual powers and for arbitrary $\delta\dot{\phi}$ and $\delta\dot{D}$, the following balance laws and the boundary conditions result [19,20]. First the macroforce balance is given by,

$$\nabla \cdot \mathbf{P} + \mathbf{b} = 0 \tag{34}$$

The microforce balance takes the form,

$$-\nabla \cdot \xi + \pi - \nabla \cdot \nabla\kappa = 0 \tag{35}$$

The boundary conditions are given by,

$$\begin{aligned} -\nabla \cdot \kappa\mathbf{n}_0 + \xi \cdot \mathbf{n}_0 + \nabla\kappa \cdot \mathbf{n}_0 = 0 \quad \text{at} \quad \partial V_0 = 0 \\ \mathbf{P}\mathbf{n}_0 = \mathbf{t} \quad \text{at} \quad \partial V_0 = 0 \\ \kappa\mathbf{n}_0 \cdot \mathbf{n}_l = 0 \quad \text{at} \quad \partial^2 V_0 = 0 \end{aligned} \tag{36}$$

4 CONSTITUTIVE THEORY

The first and the second laws of thermodynamics may be stated as follows:

$$\dot{\psi} + \eta\dot{\theta} + \dot{\eta}\theta = \mathbf{P} : \dot{\mathbf{F}} + \pi\dot{D} + \xi \cdot \nabla\dot{D} + \kappa\dot{\Delta D} - \nabla \cdot \mathbf{q} \tag{37}$$

$$\dot{\eta} + \frac{\nabla \cdot \mathbf{q}}{\theta} - \frac{\mathbf{q} \cdot \nabla \theta}{\theta^2} \geq 0 \tag{38}$$

187 Substituting the expression for $\nabla \cdot \mathbf{q}$ from Eqn. (37) in Eqn. (38), we obtain,

$$\frac{1}{\theta}\big(\mathbf{P} : \dot{\mathbf{F}} + \pi \dot{D} + \xi \cdot \nabla \dot{D} + \kappa \dot{\Delta D} - \dot{\psi} - \eta \dot{\theta}\big) - \frac{\mathbf{q} \cdot \nabla \theta}{\theta^2} \geq 0 \tag{39}$$

188 While $\mathbf{P}$, ξ and κ are all energetic π is assumed to have both energetic and dissipative com-
189 ponents; that is, $\pi = \pi_{en} + \eta_v \dot{D}$, where η_v is a viscosity parameter. The constitutive form for the
190 dissipative component ensures non-violation of the second law. The free energy and the thermo-
191 dynamic forces are assumed to have the following constitutive dependencies:

$$\begin{aligned} &\psi = \hat{\psi}(\mathbf{F}, D, \nabla D, \Delta D, \theta) \ , \mathbf{P} = \hat{\mathbf{P}}(\mathbf{F}, D, \theta) \ , \xi = \hat{\xi}(\nabla D) \ , \\ &\kappa = \hat{\kappa}(\Delta D) \ , \pi = \hat{\pi}(D) \end{aligned} \tag{40}$$

192 Using these relations, the second law may be rewritten as,

$$\begin{aligned} &\big(\mathbf{P} - \frac{\partial \psi}{\partial \mathbf{F}}\big) : \dot{\mathbf{F}} + \big(\pi_{en} - \frac{\partial \psi}{\partial \mathbf{D}}\big)\dot{D} + \big(\xi - \frac{\partial \psi}{\partial \nabla D}\big) \cdot \nabla \dot{D} \\ &+ \big(\kappa - \frac{\partial \psi}{\partial \Delta D}\big)\dot{\Delta D} - \big(\eta + \frac{\partial \psi}{\partial \theta}\big)\dot{\theta} + \eta_v (\dot{D})^2 - \frac{\mathbf{q} \cdot \nabla \theta}{\theta} \geq 0 \end{aligned} \tag{41}$$

193 The above statement of the second law gives rise to the following constitutive restrictions:

$$\mathbf{P} = \frac{\partial \psi}{\partial \mathbf{F}}; \xi = \frac{\partial \psi}{\partial \nabla D}; \kappa = \frac{\partial \psi}{\partial \Delta D}; \eta = -\frac{\partial \psi}{\partial \theta}; \pi_{en} = \frac{\partial \psi}{\partial D} \tag{42}$$

194 The heat flux assumes a Fourier form $\mathbf{q} = k_c \nabla \theta$, where k_c is a Fourier constant.

195 The constitutive forms for ξ, κ and π may be implemented in the microforce balance to yield

196 the evolution for damage.

$$\nabla \cdot \frac{\partial \psi}{\partial \nabla D} + \nabla \cdot \nabla \frac{\partial \psi}{\partial \Delta D} - \frac{\partial \psi}{\partial D} + \eta_v \dot{D} = 0 \tag{43}$$

197 The explicit forms for $\mathbf{P}, \xi, \kappa$ and π are given as follows:

$$\begin{aligned}
\mathbf{P} =& \mu(1-D)^{\frac{3}{2}}\sqrt{N}\mathscr{L}^{-1}(\overline{\Lambda}_d^r)\frac{J^{-\frac{2}{3}}}{\sqrt{3}} tr(\mathbf{F}^T\mathbf{F})^{-\frac{1}{2}}\left[\mathbf{F} - \frac{tr(\mathbf{F}^T\mathbf{F})}{3}\mathbf{F}^{-T}\right] \\
&+ \frac{K}{4}(1-D)^{\frac{3}{2}}(J^{0.5}-1)(1+\tanh\beta(J-1))J^{0.5}\mathbf{F}^{-T} \\
&+ \frac{K}{4}(J^{0.5}-1)(1+\tanh\beta(1-J))J^{0.5}\mathbf{F}^{-T} \\
&+ \frac{K}{4}(1-D)^{\frac{3}{2}}\beta(J^{0.5}-1)^2(1-\tanh^2\beta(J-1))J\mathbf{F}^{-T} \\
&- \frac{K}{4}\beta(J^{0.5}-1)^2(1-\tanh^2\beta(1-J))J\mathbf{F}^{-T}
\end{aligned} \tag{44}$$

$$\xi = \frac{18}{11\sqrt{3}} M l_R^2 \nabla D \tag{45}$$

198

$$\kappa = -\frac{12}{11\sqrt{3}} M l_R^2 (1-D) \tag{46}$$

199

$$\nabla \cdot \frac{\partial \psi}{\partial \nabla D} = \frac{18}{11\sqrt{3}} M l_R^2 \Delta D$$

200

$$\nabla \cdot \nabla \frac{\partial \psi}{\partial \Delta D} = \frac{12}{11\sqrt{3}} M l_R^2 \Delta D$$

201

$$\begin{aligned} \pi_{en} =& \frac{12}{11\sqrt{3}} \left(2MD + \Delta D\right) - \frac{3}{2}\mu(1-D)^{0.5} \\ & \left(\overline{\Lambda}_d^r \mathscr{L}^{-1}(\overline{\Lambda}_d^r) + \ln \frac{\mathscr{L}^{-1}(\overline{\Lambda}_d^r)}{\sinh(\mathscr{L}^{-1}(\overline{\Lambda}_d^r))} - f(\overline{\Lambda}_{d0}^r) \right) \\ & - \frac{3}{8} K (1-D)^{0.5} (J^{0.5}-1)^2 (1 + \tanh \beta (J-1)) \end{aligned} \tag{47}$$

202 The microforce balance results in,

$$\begin{aligned} & \frac{3}{2}(1-D)^{\frac{1}{2}} \mu \left(\overline{\Lambda}_d^r \mathscr{L}^{-1}(\overline{\Lambda}_d^r) + \ln \frac{\mathscr{L}^{-1}(\overline{\Lambda}_d^r)}{\sinh(\mathscr{L}^{-1}(\overline{\Lambda}_d^r))} - f(\overline{\Lambda}_{d0}^r) \right) \\ & + \frac{3}{8} K (1-D)^{0.5} (J^{0.5}-1)^2 \left(1 + \tanh \beta (J-1)\right) \\ & + \frac{18}{11\sqrt{3}} M l_R^2 \Delta D - \frac{24}{11\sqrt{3}} MD = \eta_v \dot{D} \end{aligned} \tag{48}$$

203 At this point, we would like draw a comparison between the microforce balance equation (48) and
204 that obtained using the second order phase field theory with quadratic degradation function similar
205 to [1],

$$\begin{aligned} & (1-D)\mu \left(\overline{\Lambda}^r \mathscr{L}^{-1}(\overline{\Lambda}^r) + \ln \frac{\mathscr{L}^{-1}(\overline{\Lambda}^r)}{\sinh(\mathscr{L}^{-1}(\overline{\Lambda}^r))} - f(\overline{\Lambda}_0^r) \right) \\ & + \frac{1}{2} K (1-D)(J^{0.5}-1)^2 \left(1 + \tanh \beta (J-1)\right) + 2 G_c l_0 \Delta D \\ & - \frac{1}{2} \frac{G_c}{l_0} D = \eta_v \dot{D} \end{aligned} \tag{49}$$

206 In this equation, $\overline{\Lambda}^r = \frac{\overline{\Lambda}}{\sqrt{N}}$, $\overline{\Lambda} = J^{-\frac{1}{3}}\frac{1}{\sqrt{3}}tr(\mathbf{C})^{1/2}$, J and $\mathbf{C}$ being the Jacobian and the right Cauchy
207 Green tensor considering that upon damage the manifold remains Euclidean. G_c and l_0 denote
208 the critical energy release rate and the regularisation length scale parameter (See [1]). The length
209 scale associated with the curvature l_R is assumed to be of the same order as the diffusion width
210 in the phase field theory l_0. Similarly, we obtain a relationship between the material constants M
211 and G_c from the Γ-convergence criteria in the next section.

212 Apart from the difference in the material constants and strain measures used for defining the
213 driving strain energy, one observe two major differences. First, the degradation function is linear in
214 the damage variable in the phase field model. Typically, this function is responsible for a decrease
215 in the driving energy contributing to the evolution of damage. In Eqn. (48), the exponent associated
216 this function is half, which might imply a delayed degradation in the driving energy vis-a-vis the
217 phase field theory. The second difference lies in the numerical factors scaling D and ΔD. The
218 coefficient of the Laplacian is a measure of ellipticity of the partial differential equation. This in
219 turn affects the converged width of the band where the curvature or damage is non-trivial as well
220 as the rate of convergence. We try to demonstrate these observations through some numerical
221 studies.

5 NUMERICAL AND ANALYTICAL STUDIES

222 To demonstrate the various features of our model for brittle fracture, we first study the analytical
223 solution to the boundary value problem introduced in Section 3.

224 5.1 Homogeneous simulations

225 We ignore all the spatial derivatives in equations Eqn. (48), thereby enforcing a homogeneous
226 distribution of stretch and damage in the system. Such an analysis has been used to investigate
227 the stress-strain response of elasto-plastic damage models in [5] and the references therein. The
228 equation for the first Piola-Kirchhoff stress and the evolution equation for the damage variable are

given by,

$$\begin{aligned}\mathbf{P} =&\mu(1-D)^{\frac{3}{2}}\mathscr{L}^{-1}(\overline{\Lambda}_d^r)\frac{J^{-1}}{3\overline{\Lambda}_d^r}\left[\mathbf{F}-\frac{tr(\mathbf{F}^T\mathbf{F})}{3}\mathbf{F}^{-T}\right]\\&+\frac{K}{4}(1-D)^{\frac{3}{2}}(J^{0.5}-1)(1+\tanh\beta(J-1))J^{0.5}\mathbf{F}^{-T}\\&+\frac{K}{4}(J^{0.5}-1)(1+\tanh\beta(1-J))J^{0.5}\mathbf{F}^{-T}\\&+\frac{K}{4}(1-D)^{\frac{3}{2}}\beta(J^{0.5}-1)^2(1-\tanh^2\beta(J-1))J\mathbf{F}^{-T}\\&-\frac{K}{4}\beta(J^{0.5}-1)^2(1-\tanh^2\beta(1-J))J\mathbf{F}^{-T}\end{aligned}\tag{50}$$

$$\begin{aligned}&\frac{3}{2}(1-D)^{\frac{1}{2}}\mu\left(\overline{\Lambda}_d^r\mathscr{L}^{-1}(\overline{\Lambda}_d^r)+\ln\frac{\mathscr{L}^{-1}(\overline{\Lambda}_d^r)}{\sinh(\mathscr{L}^{-1}(\overline{\Lambda}_d^r))}-f(\overline{\Lambda}_{d0}^r)\right)\\&+\frac{3}{8}K(1-D)^{\frac{1}{2}}(J^{0.5}-1)^2\left(1+\tanh\beta(J-1)\right)\\&-\frac{24}{11\sqrt{3}}MD=\eta_v\dot{D}\end{aligned}\tag{51}$$

Additionally, the condition for damage irreversibility is imposed through an energy history field $\mathcal{H}$ as used in [4]. The energy history field follows Kuhn-Tucker conditions [5] and is expressed as,

$$\begin{aligned}\mathcal{H}(X,t):=\max_{s\in[0,t]}&\mu\left(\overline{\Lambda}_d^r\mathscr{L}^{-1}(\overline{\Lambda}_d^r)+\ln\frac{\mathscr{L}^{-1}(\overline{\Lambda}_d^r)}{\sinh(\mathscr{L}^{-1}(\overline{\Lambda}_d^r))}-f(\overline{\Lambda}_{d0}^r)\right)\\&+\frac{K}{4}(J^{0.5}-1)^2\left(1+\tanh\beta(J-1)\right)\end{aligned}\tag{52}$$

The implicit equation in damage is thus given by,

$$\frac{3}{2}(1-D)^{\frac{1}{2}}\mathcal{H}-\frac{24}{11\sqrt{3}}MD=\eta_v\dot{D}\tag{53}$$

We choose to ignore the viscosity term for the homogeneous simulation. In that case, the closed-form solution to the above equation is given by,

$$D = \frac{11}{512\,(M)^2}\left(-33\mathcal{H}^2 + \sqrt{3}\sqrt{1024\,(M)^2\,\mathcal{H}^2 + 363\mathcal{H}^4}\right) \tag{54}$$

The corresponding expression for damage in the case of a second order phase field theory (adopted from [5]) is given by,

$$D = 1 - \left(1 + \frac{4l_0}{G_c}\mathcal{H}\right)^{-1} \tag{55}$$

with expression for stress being

$$\begin{aligned}\mathbf{P} =& \mu(1-D)^2\sqrt{N}\mathscr{L}^{-1}(\overline{\Lambda}_d^r)\frac{J^{-\frac{2}{3}}}{\sqrt{3}}tr(\mathbf{F}^T\mathbf{F})^{-\frac{1}{2}}\left[\mathbf{F} - \frac{tr(\mathbf{F}^T\mathbf{F})}{3}\mathbf{F}^{-T}\right] \\ &+ \frac{K}{4}(1-D)^2(J^{0.5}-1)(1+\tanh\beta(J-1))J^{0.5}\mathbf{F}^{-T} \\ &+ \frac{K}{4}(J^{0.5}-1)(1+\tanh\beta(1-J))J^{0.5}\mathbf{F}^{-T} \\ &+ \frac{K}{4}(1-D)^2\beta(J^{0.5}-1)^2(1-\tanh^2\beta(J-1))J\mathbf{F}^{-T} \\ &- \frac{K}{4}\beta(J^{0.5}-1)^2(1-\tanh^2\beta(1-J))J\mathbf{F}^{-T}\end{aligned} \tag{56}$$

Simulations of uniaxial tension of a hyperelastic material are carried out using both the damage theories by solving Eqs. (50) and (54) for the geometric theory and Eqs. (56) and (55) for the second order phase field theory. In comparing the two theories we assume $l_0 = l_R$ and $G_c = Ml_R$, the latter being a relation we derive later in section 5.2. The specimen is loaded, unloaded, and re-loaded. Stress and damage are assumed to be spatially homogeneous throughout the domain, and constraints in the lateral directions are provided such that $J = 1$. In both the cases, the material constants adopted are: $M = 70$N/mm^2 , $l_R = 0.1$mm, $N = 10$, $\beta = 1000$ and $\mu = 10$MPa.

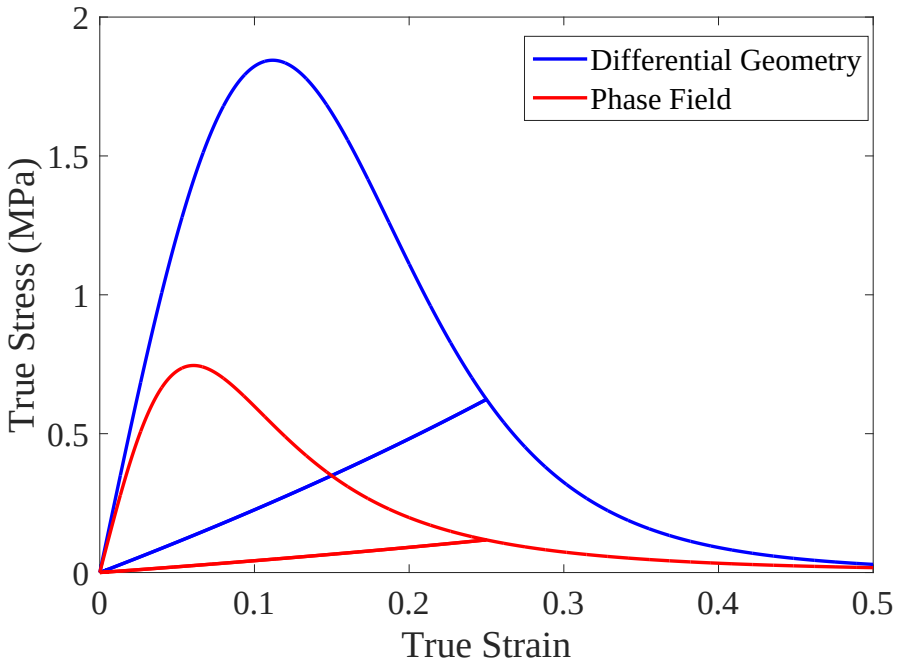

Fig. 2. Stress vs strain plot for homogeneous damage in a hyperelastic material subject to isochoric deformation; higher pre-peak degradation observed in phase field due to the quadratic degradation function

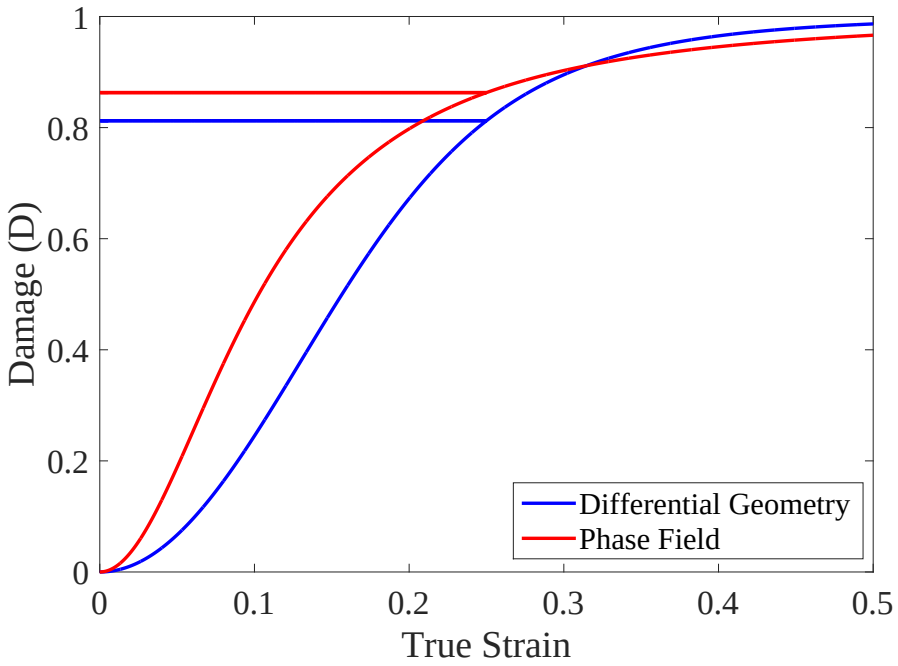

Fig. 3. Homogeneous damage evolution in a hyperelastic material subject to isochoric deformation; faster evolution is observed in the phase field theory due to a quadratic degradation function

Figures 2 and 3 clearly indicate a faster damage evolution in the second order phase-field theory and hence higher degradation at lower strains. In materials with brutal damage [3, 7], high pre-peak damage is not physically observed, even though it does occur with the second order phase field model involving a quadratic degradation function.

5.2 Inhomogeneous simulations

While homogeneous simulations afford insight into the effects of a non-quadratic degradation function, they do not furnish information on the influence of introducing a curvature based interpretation of the damage. We thus carry out a preliminary investigation through one-dimensional simulations of a bar that has developed a crack in its center when subject to a constant stretch in line with [3, 5, 9]. The above problem is posed using the following equations. The macroforce and microforce balances in one dimension may be written as,

$$\frac{\partial \sigma_P}{\partial X} = 0 \tag{57}$$

and

$$+\frac{\partial \xi}{\partial X} - \pi + \frac{\partial^2 \kappa}{\partial X^2} = 0 \tag{58}$$

where σ_p is the uniaxial stress. The one-dimensional equations for the microstresses assume the following forms,

$$\pi = \frac{12}{11\sqrt{3}} \left(2MD + Ml_R^2 \frac{\partial^2 D}{\partial X^2} \right) - \frac{3}{2} k_B n \theta (1-D)^{0.5} \mathcal{H} \tag{59}$$

$$\xi = \frac{18}{11\sqrt{3}} M l_R^2 \frac{\partial D}{\partial X} \tag{60}$$

$$\kappa = -\frac{12}{11\sqrt{3}} M l_R^2 (1 - D) \tag{61}$$

Similar to [5], we consider small deformation such that the stress is related to stretch through a linear constitutive relation $\sigma_P = E(1-D)^{\frac{3}{2}}(\lambda - 1)$. For such a case, the history variable relates to the stretch by $\mathcal{H} = \frac{1}{2}E(\lambda - 1)^2$. We also assume that the deformation is irreversible. Eqn. (57) implies that stress remains constant throughout the domain and therefore the history variable can be expressed as a function of the stress as follows:

$$\mathcal{H} = \frac{\sigma_P^2}{2E(1-D)^3} \tag{62}$$

where E is Young's modulus. The boundary conditions in 1-D may be obtained from Eqn. (36).

$$\begin{aligned} -\frac{\partial \kappa}{\partial X} + \xi + \frac{\partial \kappa}{\partial X} = 0 \quad \text{at} \quad \partial V_0 = 0 \\ \sigma_P = \mathbf{t} \quad \text{at} \quad \partial V_0 = 0 \\ \kappa = 0 \quad \text{at} \quad \partial^2 V_0 = 0 \end{aligned} \tag{63}$$

Simplifying the above expressions, the boundary conditions transform to

$$\begin{aligned} \frac{\partial D}{\partial X} = 0 \quad \text{at} \quad \partial V_0 \\ \sigma_p = \mathbf{t} \quad \text{at} \quad \partial V_0 \end{aligned} \tag{64}$$

The last boundary condition is trivially satisfied in a one-dimensional case.

The micro-force balance involving the damage variable transforms to,

$$\frac{3}{2}(1-D)^{\frac{1}{2}}\mathcal{H}+\frac{18}{11\sqrt{3}}Ml_R^2\frac{\partial^2 D}{\partial X^2}-\frac{24}{11\sqrt{3}}MD=0 \tag{65}$$

Substituting Eqn. (62) into Eqn. (65), an ordinary differential equation in the damage variable D is obtained.

$$\frac{3}{4}\frac{\sigma_P^2}{E(1-D)^{2.5}}+\frac{18}{11\sqrt{3}}Ml_R^2\frac{\partial^2 D}{\partial X^2}-\frac{24}{11\sqrt{3}}MD=0 \tag{66}$$

The damage variable at $X=0$ takes the value of unity. The damage is assumed to diffuse such that as $X\to\infty$ (i.e. far away from crack) the gradient vanishes and the phase field assumes a value of D_{hom} which is a function of the stress σ_P [9]. This results in the following far-field boundary conditions: $\frac{dD}{dX}=0$ and $D=D_{hom}$ as $X\to\infty$. The solution is symmetric about $X=0$ and differentiable at every point except at the crack tip. Note that Eqn. (66) is analytically solvable.

Similar to [5], to incorporate the far-field boundary condition and the symmetric condition, we transform the second order equation to a first order differential equation; define $W=\left(\frac{\partial D}{\partial X}\right)^2$ [21] such that Eqn. (66) can be rewritten as,

$$\frac{3}{4}\frac{\sigma_P^2}{E(1-D)^{2.5}}+\frac{18}{11\sqrt{3}}Ml_R^2\frac{\partial W}{\partial D}-\frac{24}{11\sqrt{3}}MD=0 \tag{67}$$

Solution to this equation is given by,

$$(W)^2 = \frac{0.264619\sigma_P^2}{EMl_R^2}\left(\frac{1}{(1-D_{hom})^{1.5}} - \frac{1}{(1-D)^{1.5}}\right) + \frac{(D^2 - D_{hom}^2)}{3l_R^2} \tag{68}$$

Additionally, the crack is assumed to be fully developed, so the driving stress $\sigma_P = 0$ and $D_{hom} = 0$. With these conditions, the following expressions for $\frac{\partial D}{\partial X}$ are obtained:

$$\frac{\partial D}{\partial X} = \mp\frac{D}{\sqrt{3}l_R} \tag{69}$$

Eqn. (69) is integrated from $X = 0$ to $X = \pm\infty$ with the boundary condition $D = 1$ at $X = 0$, leading to

$$D = \exp\left(\mp\frac{X}{\sqrt{3}l_R}\right) \tag{70}$$

With the phase-field model for brittle fracture [9], Γ-convergence implies that the minimizing solution to the surface energy density will converge to a minimizing solution of ψ as l_0 goes to zero. In [22], a proof of Γ-convergence is provided for the case of brittle fracture in linear elasticity, showing that as $l_0 \to 0$, the surface energy converges to the critical energy release rate G_c. For the case where $l_R = l_0$, considering that our surface energy also converges to G_c, we may derive the following relationship between M and G_c.

Substituting D from Eqn. (70) in the following expression for the surface energy,

$$\int_{-\infty}^{\infty} \psi_{R_d} dX = \int_{-\infty}^{\infty} \frac{12}{11\sqrt{3}} \left(MD^2 + Ml_R^2 \left[\frac{3}{4} \left(\frac{\partial D}{\partial X} \right)^2 - (1-D) \left(\frac{\partial^2 D}{\partial X^2} \right) \right] \right) dX \tag{71}$$

That is,

$$\int_{-\infty}^{\infty} \psi_{R_d} dX = \int_{-\infty}^{\infty} \frac{12}{11\sqrt{3}} M \left(l_R^2 \left[\frac{19}{12 l_R^2} \exp\left(\mp \frac{2X}{\sqrt{3} l_R} \right) - \frac{1}{3 l_R^2} \exp\left(\mp \frac{X}{\sqrt{3} l_R} \right) \right] \right) dX \tag{72}$$

We analytically obtain $\int_{-\infty}^{\infty} \psi_{R_d} dX = M l_R$. Thus $G_c = M l_R$.

For a partially developed crack [5], where $\sigma_P \neq 0$ and $0 < D < 1$ at $X = 0$, D_{hom} is dependent on the stress field. Moreover, the damage at $X = 0$ in fact satisfies the condition $\frac{\partial D}{\partial X} = 0$, to maintain continuity of the strain field across the damaged region. For a given value of σ_P, it is thus possible to attain a D_{center} similar to [5] from the following equation

$$\frac{0.264619\sigma^2}{E M l_R^2} \left(\frac{1}{(1-D_{hom})^{1.5}} - \frac{1}{(1-D_{center})^{1.5}} \right) + \frac{(D_{center}^2 - D_{hom}^2)}{3 l_R^2} = 0 \tag{73}$$

where D_{hom} is obtained from the following equation that is in turn obtainable via equation Eqn. (54) along with Eqn. (62) for the constant stress field:

$$\frac{\sqrt{3}\sigma_P^2}{32EM} = D_{hom}(1-D_{hom})^{2.5} \tag{74}$$

300 Similar to Eqs. (62) and (66), we may write equations for the corresponding quantities for the
301 phase-field theory

$$\mathcal{H} = \frac{\sigma_P^2}{2E(1-D)^4} \tag{75}$$

302

$$2\frac{\sigma_P^2}{E(1-D)^3} + 4G_c l_0 \frac{\partial^2 D}{\partial X^2} - \frac{G_c}{l_0} D = 0 \tag{76}$$

303 For $\sigma_P \neq 0$, the expression for the spatial gradient may be obtained as in [5],

$$\begin{aligned}\left(\frac{\partial D}{\partial X}\right)^2 =& \frac{\sigma_P^2}{2EG_c l_0}\left(\frac{1}{(1-D_{hom})^2} - \frac{1}{(1-D)^2}\right) \\ &+ \frac{(D^2 - D_{hom}^2)}{4l_0^2}\end{aligned} \tag{77}$$

304 For a fully developed crack where $\sigma_P = 0$ and $D_{hom} = 0$, the solution to the damage field is
305 given by

$$D = \exp\left(\mp\frac{X}{2l_0}\right) \tag{78}$$

306 For a partially developed crack, we may again determine D_{center} at $X = 0$ from the expression

$$\begin{aligned}&\frac{\sigma_P^2}{2EG_c l_0}\left(\frac{1}{(1-D_{hom})^2} - \frac{1}{(1-D_{center})^2}\right) \\ &+ \frac{(D_{center}^2 - D_{hom}^2)}{4l_0^2} = 0\end{aligned} \tag{79}$$

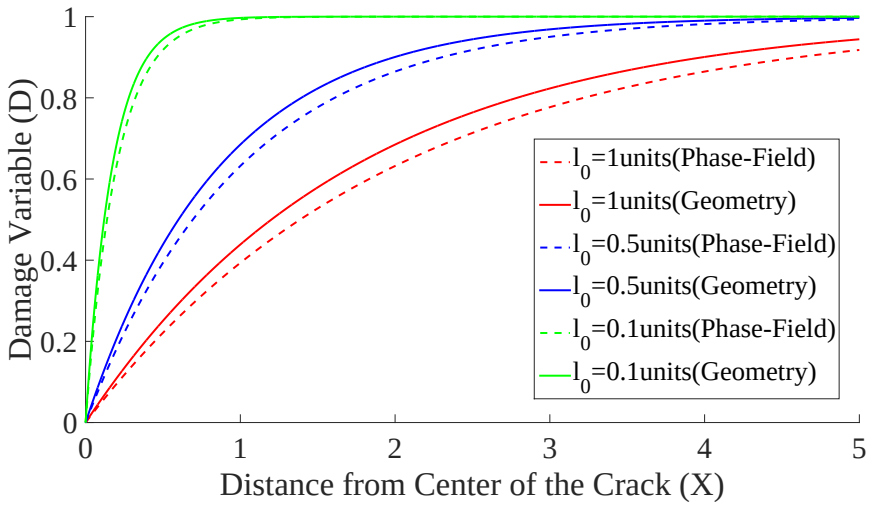

Fig. 4. Damage across the the domain for a fully developed crack at $X = 0$ for decreasing length scale l_R or l_0 for phasefield and geometry based formulation

where D_{hom} satisfies

$$\frac{2\sigma_P^2 l_0}{EG_c} = D_{hom}(1 - D_{hom})^3 \tag{80}$$

The zone of non-trivial curvature must confine to a narrower band with decreasing l_R. Such a convergence depends on the curvature based surface energy term. Analogously, with decreasing l_0, the diffused zone of damage in the phase field model must converge to a crack. We therefore do a comparison of the rates of convergence of the theories considering $l_0 = l_R$ and the relation $G_c = Ml_R$ derived from Γ-convergence.

Figure 4 shows the variation of the damage variable with distance from the crack. With decreasing value of the length scale parameter l_R or l_0, both the width of diffusion for phasefield and the zone of non-triviality of curvature in the geometric theory decrease; but the rate of decrease is faster in the geometric case. This indicates that the numerical convergence of the surface energy to Ml_R will be faster with decreasing l_R [3,9]. For a boundary value problem (of higher dimensions such as plane stress or plane strain problems) which may be solved using numerical techniques such as finite element method, this is indicative of a superior computational performance via the

k	$D_{hom,phase}$	$D_{center,phase}$	$D_{hom,geom}$	$D_{center,geom}$
0.0527	0.25	0.25	0.0029	0.8574
0.02966	0.0749	0.6512	0.00161	0.9084
0.01318	0.0288	0.8016	0.00071	0.94909
0.00329	0.0067	0.7978	0.00018	0.98054
0	0	1	0	1

Table 1. Table of D_{hom} and D_{center} for phase-field and geometric theories for various values of stress fields

geometry based model. Such a conclusion is based on the fact that convergence with l_R has a direct correlation with convergence with mesh refinement [9].

For a partially developed crack, we solve Eqs. (68) and (77) for various values of the stress field with D_{hom} and D_{center} determined through Eqs. (73), (74) and (79). Let us consider $\frac{\sigma_P^2}{EM} = k$. While Table 1 reports values of D_{center}, D_{hom} for decreasing k, figures 5 and 6 show the spatial variation of damage across the length of the bar for a partially developed crack corresponding to various values of k.

Both from Table 1 and figures 6 and 5, it may be observed that D_{hom} is the value of damage in an undamaged part of the domain. Therefore, irrespective of the stress field, its value should be 0. Similar observations may be made for D_{center} at the center of the crack which also should be independent of the extent of stress. A closer correlation with the physical scenario is clearly obtained with the geometry based formulation.

5.3 Finite element based simulation of a 2-D plane stress problem

We validate the present model against experimental results in [23] by implementing it within a finite element code in the context of a double notched styrene butadiene (SBR) plate. The finite element analysis is carried out using a program written in MATLAB 2016. Figure 7 shows the finite element representation of the problem. A plate of dimensions $200 \times 80 \times 3$mm is subjected to a quasi-statically applied displacement field of total magnitude 65.44mm. Three different lengths of the notch measuring $12mm$, $20mm$ and $28mm$ are considered. For small to moderate strains, the inverse Langevin stress approximates to the neo-Hookean stress. Since the crack extension in the

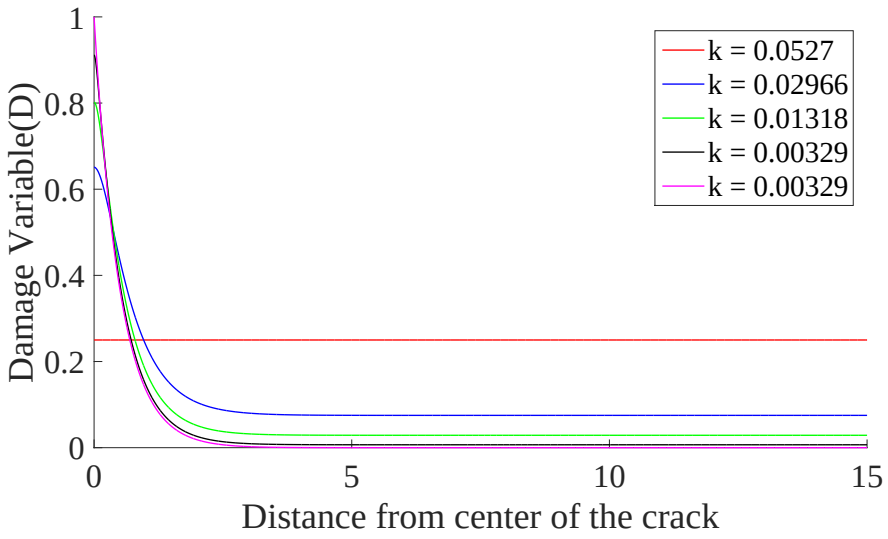

Fig. 5. Damage distribution for a partially developed crack at $X = 0$ for different stress levels with the phase field based formulation

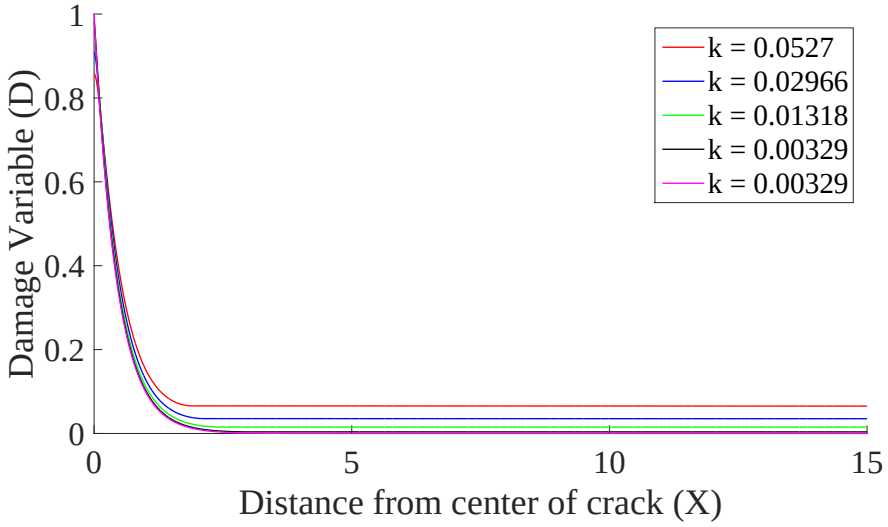

Fig. 6. Damage distribution for a partially developed crack at $X = 0$ for different stress levels with the geometry based formulation

340 experiments commences at small strains, we appropriately approximate the stress and the history
341 variable.

342 The equations for stress and the history variable are,

$$\begin{aligned}\mathbf{P} =&\mu(1-D)^{\frac{3}{2}}J^{-\frac{2}{3}}\left[\mathbf{F}-\frac{tr(\mathbf{F}^T\mathbf{F})}{3}\mathbf{F}^{-T}\right]\\&+\frac{K}{4}(1-D)^{\frac{3}{2}}(J^{0.5}-1)(1+\tanh\beta(J-1))J^{0.5}\mathbf{F}^{-T}\\&+\frac{K}{4}(J^{0.5}-1)(1+\tanh\beta(1-J))J^{0.5}\mathbf{F}^{-T}\\&+\frac{K}{4}(1-D)^{\frac{3}{2}}\beta(J^{0.5}-1)^2(1-\tanh^2\beta(J-1))J\mathbf{F}^{-T}\\&-\frac{K}{4}\beta(J^{0.5}-1)^2(1-\tanh^2\beta(1-J))J\mathbf{F}^{-T}\end{aligned}\tag{81}$$

343 and

$$\begin{aligned}\mathcal{H}(X,t):=\max_{s\in[0,t]}\frac{k_B}{2}nN\theta\left(J^{-\frac{2}{3}}tr(\mathbf{F}^T\mathbf{F})-3\right)\\+\frac{K}{4}(J^{0.5}-1)^2\left(1+\tanh\beta(J-1)\right)\end{aligned}\tag{82}$$

344 The microforce balance as a function of the history variable is thus written as,

$$\frac{3}{2}(1-D)^{\frac{1}{2}}\mathcal{H}+\frac{18}{11\sqrt{3}}Ml_R^2\Delta D-\frac{24}{11\sqrt{3}}MD=\eta_v\dot{D}\tag{83}$$

345 Before commencing with the user element, we derive the weak forms for the macroforce and
346 the microforce balances, that is, Eqs. (34) and (83), with the constitutive equation for the $\mathbf{P}$ given
347 by Eqn. (81). In the boundary value problem we consider, the displacement, hence the history
348 variable, is monotonically increased. Accordingly, the history variable in Eqn. (83) may be replaced
349 by its explicit expression in Eqn. (82).

350 Let ϕ and D be the trial functions for deformation and damage fields respectively and $\delta\phi$ and
351 δD the test functions for the macroforce and microforce balances. For a plate of thickness t, one
352 may derive the weak form of the microforce balance using the strong form in Eqn. (83) after

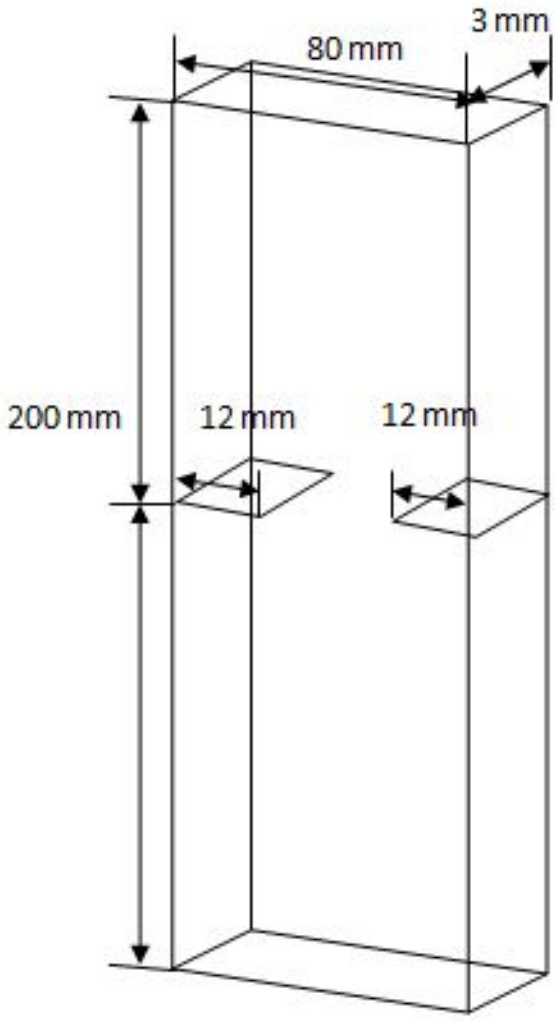

Fig. 7. Schematic Representation of the a plate with double notch [23]

353 substituting for the history variable in Eqn. (82):

$$\begin{aligned}
&\int_{A_0} \frac{3}{4}(1-D)^{\frac{1}{2}}\mu\left(J^{-\frac{2}{3}}tr(\mathbf{F}^T\mathbf{F})-3\right)\delta D \\
&+\frac{3}{8}K(1-D)^{\frac{1}{2}}(J^{0.5}-1)^2\left(1+\tanh\beta(J-1)\right)\delta D \\
&-\frac{18}{11\sqrt{3}}Ml_R^2\nabla D\delta\nabla D-\frac{24}{11\sqrt{3}}MD\delta D-\eta_v\dot{D}\delta D t dA_0=0
\end{aligned} \tag{84}$$

354 Similarly, using Eqs. (34) and (81), the weak form of the macroforce balance reads,

$$\begin{aligned}
&\int_{A_0} \mu(1-D)^{\frac{3}{2}} J^{-\frac{2}{3}} \left[\mathbf{F} - \frac{tr(\mathbf{F}^T\mathbf{F})}{3}\mathbf{F}^{-T}\right] \\
&+ \frac{K}{4}(1-D)^{\frac{3}{2}}(J^{0.5}-1)(1+\tanh\beta(J-1))J^{0.5}\mathbf{F}^{-T} \\
&+ \frac{K}{4}(J^{0.5}-1)(1+\tanh\beta(1-J))J^{0.5}\mathbf{F}^{-T} \\
&+ \frac{K}{4}(1-D)^{\frac{3}{2}}\beta(J^{0.5}-1)^2(1-\tanh^2\beta(J-1))J\mathbf{F}^{-T} \\
&- \frac{K}{4}\beta(J^{0.5}-1)^2(1-\tanh^2\beta(1-J))J\mathbf{F}^{-T} : \nabla\delta\phi t dA_0
\end{aligned} \tag{85}$$

355 Assuming bilinear approximations for both deformation and damage fields, we arrive at the
356 discretised forms for both:

$$\phi_x = \sum_{i=1}^{4} N^i \phi_{xi} \quad \phi_y = \sum_{i=1}^{4} N^i \phi_{yi} \quad D = \sum_{i=1}^{4} N^i D_i \tag{86}$$

357 where N^i are the piecewise bilinear shape functions. Correspondingly, the deformation and the
358 gradients of the damage are given by

$$\begin{aligned}
&\phi_{x,x} = \sum_{i=1}^{4} N^i_{,x}\phi_{xi} \quad \phi_{x,y} = \sum_{i=1}^{4} N^i_{,y}\phi_{xi} \quad \phi_{y,x} = \sum_{i=1}^{4} N^i_{,x}\phi_{yi} \\
&\phi_{y,y} = \sum_{i=1}^{4} N^i_{,y}\phi_{yi} \quad \nabla D_x = \sum_{i=1}^{4} N^i_{,x} D_i \quad \nabla D_y = \sum_{i=1}^{4} N^i_{,y} D_i
\end{aligned} \tag{87}$$

359 Eqs. (84) and (85) are presently solved in a staggered manner [1]; that is, the momentum
360 balance is solved for given displacement boundary conditions considering the damage value to
361 be fixed and then damage is evolved considering that the displacement does not evolve. Towards
362 this, linearisation of equations about known (discretized) displacement and damage vectors at the

363 s^{th} iteration of a nested Newton-Raphson procedure leads to

$$
\begin{aligned}
R_{\phi(s+1)} &= R_{\phi(s)} + \frac{\partial R_{\phi(s)}}{\partial \phi(s)} \Delta\phi(s) = 0 \\
R_{D(s+1)} &= R_{D(s)} + \frac{\partial R_{D(s)}}{\partial D(s)} \Delta D(s) = 0
\end{aligned}
\tag{88}
$$

364 $K_{\phi\phi} = \frac{\partial R_\phi}{\partial \phi}$ and $K_{DD} = \frac{\partial R_D}{\partial D}$ are the respective tangent stiffness matrices. The ith component of
365 the residual vector for displacement of the ath node may be determined using Eqn. (85) as follows:

$$
\begin{aligned}
R^a_{(\phi)i} = \int_{A_0} & \mu(1-D)^{\frac{3}{2}} J^{-\frac{2}{3}} \left[\mathbf{B}_{ij} - \frac{tr(\mathbf{F}^T\mathbf{F})}{3} \right] \mathbf{F}^{-1}_{mj} \\
& + \frac{K}{4}(1-D)^{\frac{3}{2}} (J^{0.5}-1)(1+\tanh\beta(J-1)) J^{0.5} \mathbf{F}^{-1}_{mi} \\
& + \frac{K}{4}(J^{0.5}-1)(1+\tanh\beta(J-1)) J^{0.5} \mathbf{F}^{-1}_{mi} \\
& + \frac{K}{4}(1-D)^{\frac{3}{2}} \beta (J^{0.5}-1)^2 (1-\tanh^2\beta(J-1)) J \mathbf{F}^{-1}_{mi} \\
& - \frac{K}{4}\beta (J^{0.5}-1)^2 (1-\tanh^2\beta(J-1)) J \mathbf{F}^{-1}_{mi} \frac{\partial N^a}{\partial X_m} t dA_0
\end{aligned}
\tag{89}
$$

366 where $\mathbf{B} = \mathbf{F}\mathbf{F}^T = \mathbf{C}^T$ is the left Cauchy-Green tensor. The residual vector for damage at the
367 same node is given by

$$
\begin{aligned}
R^a_{(D)} = \int_{A_0} & \frac{3}{4}(1-\sum_{i=1}^{4} N^b D_i)^{\frac{1}{2}} \mu \left(J^{-\frac{2}{3}} tr(\mathbf{F}^T\mathbf{F}) - 3 \right) N^a \\
& + \frac{3}{8} K (1-\sum_{i=1}^{4} N^b D_b)^{\frac{1}{2}} (J^{0.5}-1)^2 \left(1+\tanh\beta(J-1)\right) N^a \\
& - \frac{18}{11\sqrt{3}} M l_R^2 \sum_{i=1}^{4} N^b_{,x} D_b N^a_{,x} - \frac{18}{11\sqrt{3}} M l_R^2 \sum_{i=1}^{4} N^b_{,y} D_b N^a_{,y} \\
& - \frac{24}{11\sqrt{3}} M \sum_{i=1}^{4} N^b D_b N^a - \frac{\eta_v}{\tau} \sum_{i=1}^{4} N^b (D_b^{s+1} - D_b^s) N^a t dA_0
\end{aligned}
\tag{90}
$$

The above residual vectors are used in Eqs. 88. The tangent stiffness matrices for deformation and damage are respectively given by

$$K_{(\phi\phi)aibk} = \int_{A_0} \frac{\partial N^a}{\partial X_j} \frac{\partial \mathbf{P}_{ij}}{\partial \mathbf{F}_{kl}} \frac{\partial N^b}{\partial X_l} t dA_0 \tag{91}$$

$$\begin{aligned} K_{(DD)ab} = & \int_{A_0} \frac{3}{8}(1-\sum_{p=1}^{4} N^p D_p)^{-\frac{1}{2}} \mu \left(J^{-\frac{2}{3}} tr(\mathbf{F}^T\mathbf{F}) - 3 \right) N^a N^b \\ & + \frac{3}{16} K (1-\sum_{p=1}^{4} N^p D_p)^{-\frac{1}{2}} (J^{0.5}-1)^2 \left(1+\tanh\beta(J-1)\right) N^a N^b \\ & + \frac{18}{11\sqrt{3}} M l_R^2 N^a_{,x} N^b_{,x} + \frac{18}{11\sqrt{3}} M l_R^2 N^a_{,y} N^b_{,y} + \frac{24}{11\sqrt{3}} M N^a N^b \\ & + \frac{\eta_v}{\tau} N^b N^a t dA_0 \end{aligned} \tag{92}$$

For the sake of brevity, we do not provide an explicit expression for $\frac{\partial \mathbf{P}_{ij}}{\partial \mathbf{F}_{kl}}$ in this manuscript.

The set of discretized non-linear equations for displacement and damage fields is solved using a modified Newton–Raphson method. The relaxation factor used in the modified Newton–Raphson scheme is kept at a sufficiently low value to enable a convergent solution to the non-linear set of discretized equations [24]. The simulations are performed in a monotonic displacement-driven context. Two different sets of time increments and relaxation factors are used. A displacement increment of 0.64 and a relaxation factor of 1 are used when the damage at any nodal point in the model reaches 0.4 After that, the displacement increment is reduced to 0.001, and the relaxation factor is reduced to 0.01. A cutback scheme is used to successively reduce the time step when the damage reaches 0.96 to capture brutal failure. Elements with a phase field value greater than 0.96 are considered to have negligible stiffness and they are not shown. The code is parallelized using the in-built functionality of MATLAB to speed up the simulation process. Vectorized versions of stiffness matrix assembly is implemented using an algorithm given in [25].

The material constants are assumed to have the following values: μ = 0.19 MPa and the

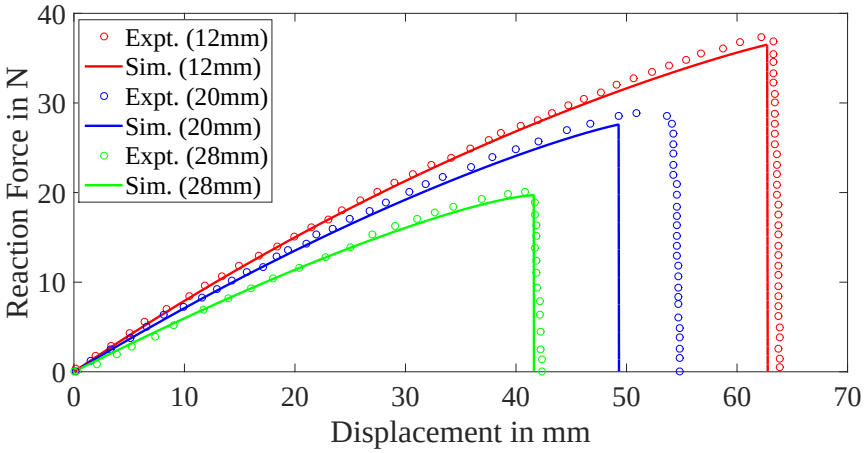

Fig. 8. Comparison of experiments with simulation for double notch [23]

Poisson's ratio to be 0.45. The size of the smallest element in the mesh is taken to be 0.5mm and and M and the length scale parameter l_R are 0.95 N/mm^2 and 2 mm respectively.

Figure 8 shows a comparison of the results obtained from simulation and experiment [23]. The peak loads and the failure displacement compare well for the notch sizes 28 mm and 12 mm. Figure 9 shows the contour of the damage variable on the deformed geometry for various top edge displacements of the plate with a notch size of 28mm. For 20 mm notch size, we observe a deviation from the experimental data which is not unusual if we refer to the comparisons reported in [10] and [1]. This discrepancy might be attributed to errors in carrying out experiments.

CONCLUSIONS

Based on the postulate that damage induces a Riemannian curvature in the material manifold, we have proposed a model for brittle damage in compressible elastomers. The changeover from an Euclidean to a Riemannian manifold results in damage-dependent length, area and volume measures and is also reflected in stiffness degradation and the energy created due to new surfaces. The energy is assumed to be a function of the Riemannian curvature. Thanks to the geometric moorings of our damage model, the extent of degradation prior to peak load is significantly reduced vis-á-vis the conventional second order phase-field theory with a quadratic degradation function. The introduction of curvature-dependent surface energy also leads to a superior compu-

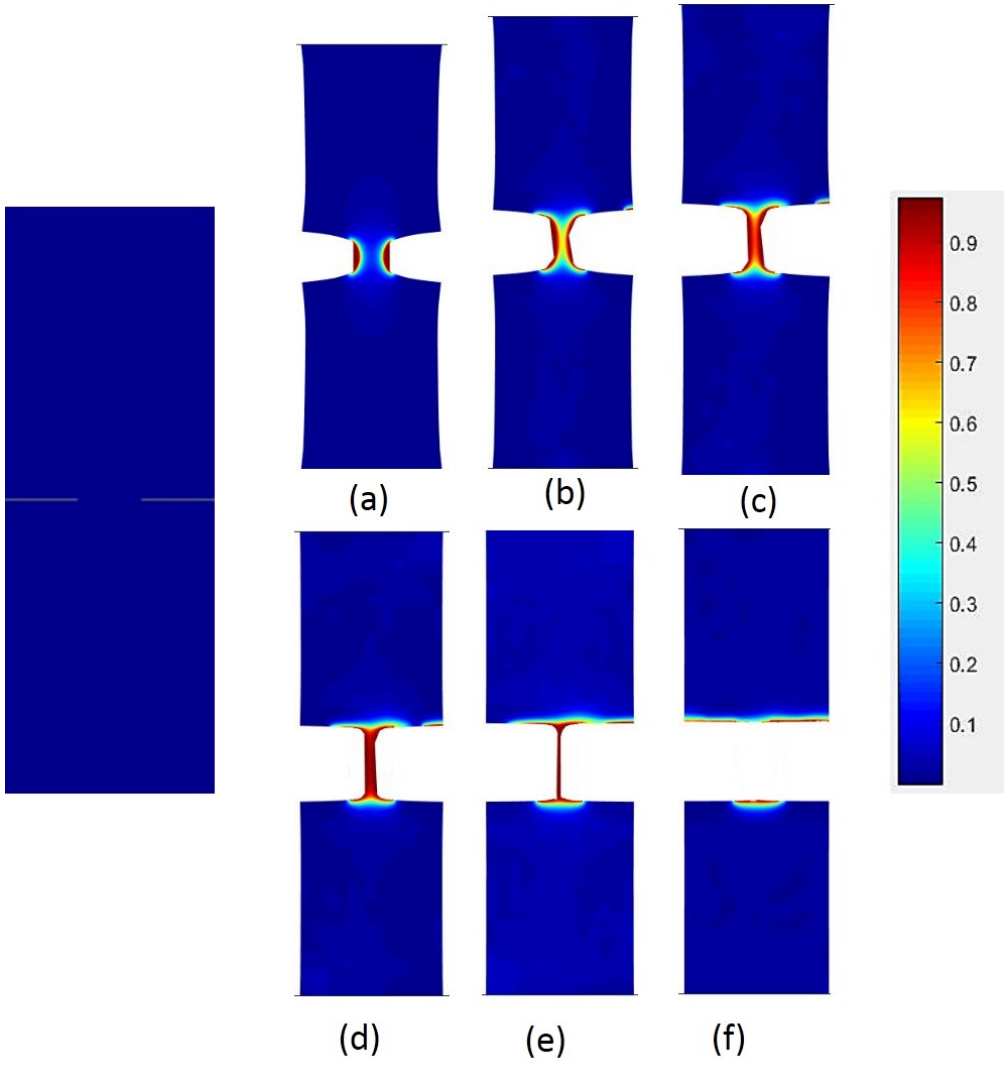

Fig. 9. Damage contour at displacements of a)20mm b)41.601mm c)41.607mm d)41.610mm e)41.617mm f) 41.624mm (displacements of the topmost edge of the plate)

tational performance. Using finite element discreization, we have also used the model to solve the problem of a double notched plate subject to tension. We have considered three different notch sizes and compared the results with experimental observations as in [23]. The contour shows the gradual extension of the damage in line with numerical studies conducted in [1]. We also anticipate that the convergence with mesh size in the plane stress simulation will be faster following a demonstration of superior convergence with l_R in the one-dimensional case. This correlation between the convergence rates in one-dimensional and plane stress simulations has been noted

in [9]. We have however not been able to explicitly demonstrate the faster convergence through our simulations on the double notched plate as high non-linearity rapidly sets in when damage starts to propagate and it is difficult to record the surface energy for comparing with the parameter G_c.

In future, we intend to use this model to conduct three dimensional finite element simulations and also extend the framework to include incompressible materials.

ACKNOWLEDGEMENTS

All authors are thankful to Indian Space Research Organisation for funding this research. The last author acknowledges the support from the NSF (CMMI) award (FAIN) 1952873.

REFERENCES

[1] Miehe, C., and Schänzel, L.-M., 2014. "Phase field modeling of fracture in rubbery polymers. part i: Finite elasticity coupled with brittle failure". *Journal of the Mechanics and Physics of Solids,* **65**, pp. 93–113.

[2] Jirásek, M., 2004. "Non-local damage mechanics with application to concrete". *Revue française de génie civil,* **8**(5-6), pp. 683–707.

[3] Goswami, S., Anitescu, C., and Rabczuk, T., 2020. "Adaptive fourth-order phase field analysis for brittle fracture". *Computer Methods in Applied Mechanics and Engineering,* **361**, p. 112808.

[4] Miehe, C., Hofacker, M., and Welschinger, F., 2010. "A phase field model for rate-independent crack propagation: Robust algorithmic implementation based on operator splits". *Computer Methods in Applied Mechanics and Engineering,* **199**(45-48), pp. 2765–2778.

[5] Borden, M. J., Verhoosel, C. V., Scott, M. A., Hughes, T. J., and Landis, C. M., 2012. "A phase-field description of dynamic brittle fracture". *Computer Methods in Applied Mechanics and Engineering,* **217**, pp. 77–95.

[6] Bourdin, B., Francfort, G. A., and Marigo, J.-J., 2008. "The variational approach to fracture". *Journal of elasticity,* **91**(1-3), pp. 5–148.

[7] Sargado, J. M., Keilegavlen, E., Berre, I., and Nordbotten, J. M., 2018. "High-accuracy phase-field models for brittle fracture based on a new family of degradation functions". *Journal of the Mechanics and Physics of Solids,* **111**, pp. 458–489.

[8] Tanné, E., Li, T., Bourdin, B., Marigo, J.-J., and Maurini, C., 2018. "Crack nucleation in variational phase-field models of brittle fracture". *Journal of the Mechanics and Physics of Solids,* **110**, pp. 80–99.

[9] Borden, M. J., Hughes, T. J., Landis, C. M., and Verhoosel, C. V., 2014. "A higher-order phase-field model for brittle fracture: Formulation and analysis within the isogeometric analysis framework". *Computer Methods in Applied Mechanics and Engineering,* **273**, pp. 100–118.

[10] Tang, S., Zhang, G., Guo, T. F., Guo, X., and Liu, W. K., 2019. "Phase field modeling of fracture in nonlinearly elastic solids via energy decomposition". *Computer Methods in Applied Mechanics and Engineering,* **347**, pp. 477–494.

[11] Ye, J.-Y., Yin, B.-B., Zhang, L.-W., and Reddy, J., 2020. "Large strained fracture of nearly incompressible hyperelastic materials: enhanced assumed strain methods and energy decomposition". *Journal of the Mechanics and Physics of Solids*, p. 103939.

[12] Borden, M. J., Hughes, T. J., Landis, C. M., Anvari, A., and Lee, I. J., 2016. "A phase-field formulation for fracture in ductile materials: Finite deformation balance law derivation, plastic degradation, and stress triaxiality effects". *Computer Methods in Applied Mechanics and Engineering,* **312**, pp. 130–166.

[13] Miehe, C., Göktepe, S., and Lulei, F., 2004. "A micro-macro approach to rubber-like materialspart i: the non-affine micro-sphere model of rubber elasticity". *Journal of the Mechanics and Physics of Solids,* **52**(11), pp. 2617–2660.

[14] Murakami, S., 1988. "Mechanical modeling of material damage". *Journal of Applied Mechanics,* **55**, pp. 280–286.

[15] Lemaitre, J., 1985. "A continuous damage mechanics model for ductile fracture". *Journal of Engineering Materials and Technology,* **107**, pp. 83–89.

[16] Steinmann, P., and Carol, I., 1998. "A framework for geometrically nonlinear continuum damage mechanics". *International Journal of Engineering Science,* **36**(15), pp. 1793–1814.

[17] Rastiello, G., Giry, C., Gatuingt, F., and Desmorat, R., 2018. "From diffuse damage to strain localization from an eikonal non-local (enl) continuum damage model with evolving internal length". *Computer Methods in Applied Mechanics and Engineering,* **331**, pp. 650–674.

[18] Arruda, E. M., and Boyce, M. C., 1993. "A three-dimensional constitutive model for the large stretch behavior of rubber elastic materials". *Journal of the Mechanics and Physics of Solids,* **41**(2), pp. 389–412.

[19] Frémond, M., and Nedjar, B., 1996. "Damage, gradient of damage and principle of virtual power". *International journal of solids and structures,* **33**(8), pp. 1083–1103.

[20] Duda, F. P., Ciarbonetti, A., Sánchez, P. J., and Huespe, A. E., 2015. "A phase-field/gradient damage model for brittle fracture in elastic–plastic solids". *International Journal of Plasticity,* **65**, pp. 269–296.

[21] Zaitsev, V. F., and Polyanin, A. D., 2002. *Handbook of exact solutions for ordinary differential equations*. Chapman and Hall/CRC.

[22] Chambolle, A., 2004. "An approximation result for special functions with bounded deformation". *Journal de mathématiques pures et appliquées,* **83**(7), pp. 929–954.

[23] Hocine, N. A., Abdelaziz, M. N., and Imad, A., 2002. "Fracture problems of rubbers: J-integral estimation based upon η factors and an investigation on the strain energy density distribution as a local criterion". *International Journal of Fracture,* **117**(1), pp. 1–23.

[24] Fujiwara, K., Nakata, T., Okamoto, N., and Muramatsu, K., 1993. "Method for determining relaxation factor for modified newton-raphson method". *IEEE transactions on magnetics,* **29**(2), pp. 1962–1965.

[25] Cuvelier, F., Japhet, C., and Scarella, G., 2013. "An efficient way to perform the assembly of finite element matrices in matlab and octave". *arXiv preprint arXiv:1305.3122*.

LIST OF FIGURES

LIST OF TABLES